

INTERACTION OF LASER RADIATION WITH MATTER

PACS numbers: 42.55.Lt; 42.65.Ky; 52.35.Tc; 79.20.Ds
DOI: 10.1070/QE2013v043n07ABEH014765

Numerical analysis of experiments on the generation of shock waves in aluminium under indirect (X-ray) action on the Iskra-5 facility

S.V. Bondarenko, G.V. Dolgoleva, E.A. Novikova

Abstract. **The dynamics of laser and X-ray radiation fields in experiments with cylindrical converter boxes (illuminators), which had earlier been carried out on the Iskra-5 laser facility (the second harmonic of iodine laser radiation, $\lambda = 0.66$ μm) was investigated in a sector approximation using the SND-LIRA numerical technique. In these experiments, the X-ray radiation temperature in the box was determined by measuring the velocity of the shock wave generated in the sample under investigation, which was located at the end of the cylindrical illuminator. Through simulations were made using the SND-LIRA code, which took into account the absorption of laser driver radiation at the box walls, the production of quasi-thermal radiation, as well as the formation and propagation of the shock wave in the sample under investigation. An analysis of the experiments permits determining the electron thermal flux limiter f: for $f = 0.03$ it is possible to match the experimental scaling data for X-ray in-box radiation temperature to the data of our simulations. The shock velocities obtained from the simulations are also consistent with experimental data. In particular, in the experiment with six laser beams (and a laser energy $E_L = 1380$ J introduced into the box) the velocity of the shock front (determined from the position of a laser mark) after passage through a 50-μm thick base aluminium layer was equal to 35±1.6 km s^{-1}, and in simulations to 36 km s^{-1}. In the experiment with four laser beams (for $E_L = 850$ J) the shock velocity (measured from the difference of transit times through the base aluminium layer and an additional thin aluminium platelet) was equal to 30±3.6 km s^{-1}, and in simulations to 30 km s^{-1}.**

Keywords: *shock waves, indirect X-ray action, iodine laser, numerical simulations.*

1. Introduction

For many years the Iskra-5 laser facility has been employed to carry out experiments on irradiation of targets of different type with the aim to experimentally investigate the properties of matter and radiation at high temperatures. The data of experimental investigations of shock wave (SW) generation in plane samples loaded by quasi-thermal radiation were outlined in Ref. [1]. To date, the Iskra-5 facility permits performing experiments at a laser radiation wavelength $\lambda = 0.66$ μm for a total input laser energy of 2–3 kJ and a subnanosecond duration of the laser pulse.

In the laser-to-X-ray radiation conversion experiments conducted, use was made of 0.9-mm-long cylindrical boxes 0.6 mm in diameter (Fig. 1), with their inner surface coated with gold. Laser beams were introduced through openings 300 μm in diameter. A screen (*3*) was mounted for shielding from direct laser beams and their reflexes, as well as from plasma radiation. The loaded samples were aluminium foils with step-like coatings of different materials. Two-to-eight laser beams with a radiation wavelength of $\lambda = 0.66$ μm, pulse lengths of $\tau_{1/2} = 0.3$–0.5 ns and a total energy of 500–2000 J were introduced into the converter box.

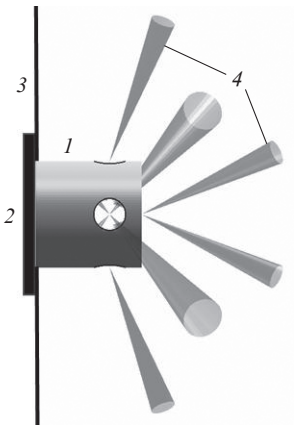

Figure 1. Structure of the target irradiated by six beams: (*1*) converter box; (*2*) radiation-bearing (loaded) sample; (*3*) light shield; (*4*) laser beams.

One of the tasks in indirect (X-ray) irradiation experiments on high-power laser facilities is to determine the temperature of quasi-equilibrium X-ray radiation in the box. This may be done by measuring the SW velocity in the radiation-bearing (loaded) sample, provided the equation of state of the check sample is sufficiently well known for the experimental conditions involved. In this case, the measured SW velocity is used to calculate the pressure on the sample and the effective temperature of the heating radiation.

To interpret experiments in Ref. [1] advantage was taken of a computation-based scaling which permitted determining the SW velocity from the known radiation temperature. However, of obvious interest is the problem of through simu-

S.V. Bondarenko, E.A. Novikova Russian Federal Nuclear Centre – All-Russian Research Institute of Experimental Physics, prosp. Mira 37, 607190 Sarov, Nizhnii Novgorod region, Russia;
e-mail: sergvicbond@inbox.ru, novikova@md08.vniief.ru;
G.V. Dolgoleva M.V. Keldysh Institute for Applied Mathematics, Russian Academy of Sciences, Miusskaya pl. 4, 125047 Moscow, Russia; e-mail: dolgg@list.ru

Received 6 November 2011; revision received 3 February 2013
Kvantovaya Elektronika **43** (7) 630–637 (2013)
Translated by E.N. Ragozin

lations, when both the radiation temperature and the SW parameters in the sample under investigation are determined from the simulation data for the dynamics of the radiation fields in the laser target converter box. The input data for such simulations are only the characteristics of laser driver radiation and the structure of the target itself.

Our simulations were carried out using the SND-LIRA numerical technique [2, 3], which permits calculating in a sector approximation and a three-dimensional formulation the propagation and absorption of laser radiation as well as the production and transfer of X-ray radiation in the inner volume of a quasi-closed converter box. In the execution of these simulations under this approximation, the box surface is divided into gas-dynamically uncoupled domains (sectors). One-dimensional (sector) numerical simulations are used to determine the plasma state at the walls of the converter box. Furthermore, employed in the SND-LIRA code are three-dimensional algorithms for calculating the transfer of laser and X-ray radiation fields inside the box using the Monte-Carlo technique with convergence acceleration for integral sums [4]. The unification of these approaches in the framework of one numerical technique permits carrying out the numerical simulations of the three-dimensional structures of laser target boxes.

To specify the spatial and angular characteristics of laser radiation, each beam was represented as a statistical collection of individual rays, which propagate independently according to the laws of geometrical optics. The resultant illumination structure was calculated by summation of the contributions of individual rays. The absorption of laser radiation was calculated for the temperature and density profiles in the near-wall plasma obtained in one-dimensional simulations. In this case, a part of the laser radiation flux may experience specular reflection from the inner box surface to fall once again on the wall of the converter box or scatter through the openings.

Earlier we had performed numerical simulations of experiments with spherical converter boxes with the use of the second iodine laser harmonic [3], including boxes with different material coatings of the walls [5]. These simulations showed the necessity to accurately describe the electron heat transfer in the volume of the resultant near-wall plasma. The electron thermal flux limiter f, which defines the maximum fraction of the total kinetic energy flux that may be transferred by the electrons, turns out to be the critical parameter in the modelling of these experiments. The action of focused laser radiation produces strong electron temperature gradients in the near-wall plasma. To describe the heat transfer in the hot nonequilibrium plasma, advantage may not be taken of the classical relations obtained by Spitzer [6] under the assumption that the electron free path is much shorter than the characteristic temperature gradient scale length. To avoid a non-physical situation, Malone et al. [7] came up with the idea of limiting the heat flux q transferred by the electrons to a fraction of the free-streaming limit:

$$q = f k_B T_e v_e, \tag{1}$$

where T_e is the electron temperature; k_B is the Boltzmann constant; v_e is the thermal electron velocity; and $f \sim 0.65$. It turned out that matching experimental data to the data of simulations required lowering f to the values $0.03 \leqslant f \leqslant 0.1$ [7–9].

The introduction of a stronger limiting factor (i.e. for small f) results in the uncontrolled effect of heat in the inner box volume accessible to laser radiation propagation (this plasma domain with densities below the critical density for the given optical radiation wavelength will be hereinafter referred to as the laser corona). In this case, discontinuities in electron temperature profiles may emerge in the numerical solution. This leads to the following two consequences. First, the stronger limitation gives rise to an overheat of the laser corona, resulting in a lowering of the inverse-bremsstrahlung absorption coefficient k_a (in μm^{-1}) for laser radiation according to the expression

$$k_a = 100 \frac{\bar{Z}\overline{Z^2}}{A^2} \frac{\rho \lambda_0^2}{T_e^{5/2}}, \tag{2}$$

where $\bar{Z}$ and $\overline{Z^2}$ are the average charge and the average squared charge of the plasma ions; A is the atomic number; ρ is the density; and λ_0 is the wavelength of laser radiation (in μm). Second, the limitation of heat transfer to the denser supercritical plasma layers (which will be hereinafter referred to as the X-ray corona) lowers the temperature of X-ray radiation generated at the box walls. It is noteworthy that a similar numerical technique was developed for interpreting the experiments on indirect irradiation of targets with a spherical geometry of converter boxes, which were carried out on the OMEGA laser facility [10].

Using the SND-LIRA code, our simulations were made for two f values, which bound the specified range and correspond to the cases of weak ($f = 0.1$) and strong ($f = 0.03$) limitation. A one-dimensional simulation by the SND code [11] was performed in each sector problem. The following physical processes were included: plasma motion in the two-temperature approximation, electron and ion heat conductivities with electron–ion relaxation, X-ray radiation transfer in the spectral multigroup diffusion approximation (100 spectral groups uniformly distributed over the 0–5 keV interval). The ionisation kinetics of the plasma, the spectral paths in it and its radiative characteristics , as well as the equations of state were calculated from the averaged ion model [11] with the inclusion of the splitting of atomic and ionic energy states in the orbital quantum number (splitting in l).

Prior to the execution of detailed simulations, useful information can be gained from the calculations of laser radiation absorption at the box walls on defining a model dependence of the absorption coefficient on the angle γ of radiation incidence on the surface in the form

$$k_a = k_0 \cos^3 \gamma. \tag{3}$$

For the conditions of irradiation at the second harmonic frequency of the iodine laser ($\lambda = 0.66$ μm) we take $k_0 = 1$. In these calculations the box walls are assumed to be immobile and the shape of the reflecting surface is assumed to be invariable.

2. Results of simulations

Figure 2 shows the structure of laser irradiation of the inner illuminator surface obtained in simulations with a model absorption coefficient (3) for different numbers of laser beams involved. The two-beam experiment scheme implies the input of two beams through the opening in the end face. Four beams are injected through the four openings in the cylindrical illuminator surface. The use of six beams permits implementing the scheme of combined illuminator irradiation through the opening in the end face (two beams) and four side openings. Lastly, we consider the version of illuminator irradiation by

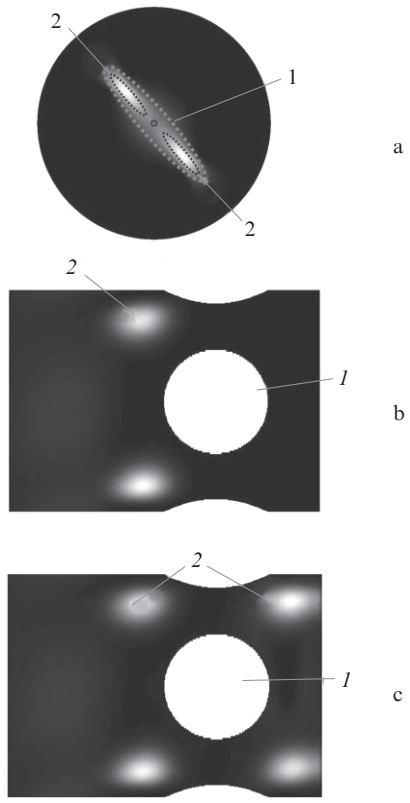

Figure 2. Secondary laser irradiation pattern on the illuminator end, which is formed due to the specular reflection of two laser beams, which are introduced through the end opening, from the cylindrical illuminator surface (1 – a lower-intensity irradiation zone in the form of an ellipse with semiaxes $A = 0.215$ mm and $B = 0.050$ mm, 2 – a higher-intensity irradiation zone in the form of two ellipses with semiaxes $a = 0.069$ mm and $b = 0.023$ mm) (a) and pattern of the primary irradiation of the cylindrical illuminator surface by four (b) and eight (c) laser beams introduced through the four openings in the side illuminator surface [(*1*) openings, (*2*) primary laser irradiation spots].

eight beams introduced through the four openings in the cylindrical illuminator surface. The structure of the illuminator itself was the same in all these cases.

When two laser beams are injected through the opening in the end face of the illuminator, the optical radiation is incident on the cylindrical illuminator surface at angles of ~60°, with the consequence that the absorption in the primary laser spots turns out to be low. In this case, the reflection of light from the cylindrical mirror results in the formation of high-intensity secondary irradiation zones on the illuminator ends (see Fig. 2a). The laser radiation is incident on the illuminator end at angles of ~30°, which substantially increases the absorption in the secondary laser spots [according to formula (3)].

Figure 2b shows the pattern of laser irradiation of the inner illuminator surface produced by four laser beams introduced through the four openings in the side (cylindrical) illuminator surface. In this method of injecting laser energy, its major fraction is absorbed in the primary irradiation spots and the scattered radiation intensity turns out to be low. When six beams are used, the distribution of laser irradiance of the inner illuminator surface may be represented as the 'sum' of the distributions depicted in Figs 2a and 2b. Figure 2c shows the laser irradiance of the side illuminator surface by eight laser beams introduced through the four openings in its side surface. (In this case, formed on the cylindrical illuminator surface is a laser irradiation pattern with eight primary laser spots.)

We note that the plasma motion in the primary spot region, considering the side expansion of the plasma and the nonuniformity of laser irradiation, distorts the cylindrical shape of the reflecting surface of the plasma ablated from the illuminator walls, with the result that the secondary laser irradiation zone depicted in Fig. 2a will be larger (and the irradiation intensity will be lower). The data of simulations for these domains must be treated as an upper estimate of the possible effect of laser radiation absorption in them.

An analysis of laser irradiation pattern performed for our model simulations with the absorption coefficient defined by formula (3) permits partitioning the inner illuminator surface into gas-dynamically unconnected domains – sectors, this partitioning being adequate to the experimental situation. Individual sectors corresponded to primary irradiation zones as well as to illuminator ends. In secondary laser irradiation zones we singled out two domains with different laser irradiances (see Fig. 2a). The cylindrical illuminator surface beyond the laser irradiation spots was united in one sector.

The box wall in the zones of primary laser spots experiences strong heating due to absorption of high-intensity laser radiation. An advance substance dynamics is observed here, which leads to violation of the cylindrical geometry of the gas-dynamic motion in these domains. Prescribing the one-dimensional cylindrical simulation geometry in them would have imposed a physically unreasonable regime of gas-dynamic motion with the subsequent plasma collapse on the cylinder axis. That is why hereinafter the simulations for the zones of primary laser irradiation were performed under a plane geometry approximation in the unlimited plasma expansion from the box walls. We emphasise that this approximation does not permit including several effects: the side expansion of the plasma ablated in the laser irradiation spots as well as the effect of heat transfer along the box wall. Consistent inclusion of these effects will require a full-scale three-dimensional gas-dynamic simulation.

The SND-LIRA numerical technique was used to calculate the dynamics of laser and X-ray radiation fields inside a cylindrical illuminator for the electron thermal flux limiter $f = 0.1$ and 0.03 in the substance of the box walls. The energy of each laser beam was assumed to be equal to 250 J for a laser pulse duration $\tau_{1/2} = 0.5$ ns at a wavelength $\lambda = 0.66$ μm. (Increasing the number of beams accordingly increases the total amount of laser energy injected into the box.)

Tables 1–4 show the calculated data which characterise the conditions for all portions (sectors) of the inner illuminator surface in simulations with different numbers N of laser beams ($N = 2, 4, 6, 8$). One can see to what extent the absorbed laser energy depends on the f factor.

The results of simulations of the dynamics of laser radiation absorption in a spherical converter box, the radiance temperature variations of the box walls, and the box emission spectra, which were performed using the SND-LIRA numerical technique, were considered at length in Ref. [5]. No significant changes are observed in going over to the cylindrical box geometry (perhaps with the exception of the two-beam illuminator irradiation scheme, when a significant fraction of laser energy is absorbed at the aluminium end face, and not at the gold-coated box walls). We therefore refer the reader to Ref. [5] and, in the framework of the present paper, restrict ourselves to the data collected in the tables.

Table 1. Calculated characteristics of laser radiation absorption and quasi-equilibrium X-ray radiation generated at the inner surface of a cylindrical illuminator under irradiation by two laser beams.

Sector No.	E_{las}/J		$\langle I_a \rangle/10^{14}$ W cm^{-2}		$\langle \eta \rangle$		T_X/eV		Sector positions
	$f = 0.1$	$f = 0.03$	$f = 0.1$	$f = 0.03$	$f = 0.1$	$f = 0.03$	$f = 0.1$	$f = 0.03$	
0	81	183					115	98	Openings
1	44	26	0.65	0.39	0.14	0.07	142	112	Primary laser spots on cylindrical surface
2	44	26	0.63	0.39	0.14	0.07	142	112	
3	73	88	0.57	0.69	0.69	0.41	145	129	Au end face
4	142	97	0.99	0.68	0.74	0.4	124	100	Al end face
5	21	25	0.034	0.041	0.23	0.13	112	96	Cylindrical surface beyond primary spots
6	64	37	5.5	3	0.31	0.16	178	131	Al end face in the domain of secondary laser irradiation (zone 1 in Fig. 2a)
7	32	19	6.5	4	0.29	0.16	188	137	Al end face in the domain of secondary laser irradiation (zone 2 in Fig. 2a)
	$E_L = 501$ J	$E_L = 502$ J							

Notes: E_{las} is the laser radiation energy absorbed on the sector surface; $\langle I_a \rangle$ and $\langle \eta \rangle$ are the absorbed laser intensity and absorbed energy fraction averaged over the course of the laser pulse; and T_X is temperature at the peak of luminosity of the box wall.

Table 2. Same as in Table 1, with illuminator irradiation by four beams.

Sector No.	E_{las}/J		$\langle I_a \rangle/10^{14}$ W cm^{-2}		$\langle \eta \rangle$		T_X/eV		Sector positions
	$f = 0.1$	$f = 0.03$	$f = 0.1$	$f = 0.03$	$f = 0.1$	$f = 0.03$	$f = 0.1$	$f = 0.03$	
0	4.1	37					165	157	Openings
1	205	136	5.3	3.5	0.73	0.4	225	185	Primary spots on cylindrical illuminator surface
2	184	118	4.8	3.1	0.66	0.35	225	185	
3	184	118	4.8	3.1	0.66	0.35	225	185	
4	205	136	5.3	3.5	0.73	0.41	225	185	
5	0.068	0.95	0.0005	0.0075	*	*	150	150	Au end face
6	2.9	3.2	0.02	0.022	*	*	127	125	Al end face
7	218	454	0.36	0.75	0.85	0.56	166	172	Cylindrical surface beyond primary spots
8	0.38	0.26	0.032	0.022	*	*	127	125	Al end face
9	0.2	0.19	0.041	0.038	*	*	127	125	
	$E_L = 1003$ J	$E_L = 1003$ J							

*The value of absorption coefficient is not given owing to the smallness of absorbed laser energy.

Table 3. Same as in Table 1, with illuminator irradiation by six beams.

Sector No.	E_{las}/J		$\langle I_a \rangle/10^{14}$ W cm^{-2}		$\langle \eta \rangle$		T_X/eV		Sector positions
	$f = 0.1$	$f = 0.03$	$f = 0.1$	$f = 0.03$	$f = 0.1$	$f = 0.03$	$f = 0.1$	$f = 0.03$	
0	94	208					172	158	Openings
1	11	7.4	5.5	3.8	0.71	0.43	224	186	Primary spots of irradiation by beams introduced through openings in the side surface
2	184	117	4.8	3	0.71	0.43	224	186	
3	184	117	4.8	3	0.71	0.43	224	186	
4	11	7.4	5.5	3.8	0.71	0.43	224	186	
5	42	51	1.3	1.6	0.31	0.25	186	170	Primary spots of irradiation by beams introduced through opening in the end face
6	42	51	1.3	1.6	0.31	0.25	186	170	
7	212	144	5.7	3.9	0.47	0.27	229	190	Domains of overlapping of primary spots
8	211	143	5.7	3.9	0.47	0.27	229	190	
9	77.6	95	0.62	0.76	0.83	0.49	171	165	Au front end face
10	140	100	0.98	0.7	0.58	0.24	152	136	Al rear end face
11	197	410	0.36	0.76	0.66	0.51	172	171	Cylindrical surface beyond primary spots
12	67	35	5.6	3	0.34	0.16	193	153	Al end face in secondary irradiation region (zone 1 in Fig. 2a)
13	31	19	6.3	3.8	0.33	0.15	193	153	Al end face in secondary irradiation region (zone 2 in Fig. 2a)
	$E_L = 1504$ J	$E_L = 1504$ J							

Among the results of the present work is the determination of the electron thermal flux limiter f, which permits matching the data of numerical simulations to the results of measurements of the effective X-ray radiation temperature in the box. The best agreement is reached for $f = 0.03$. That is why, to spare space and the reader's time, all results in the

Table 4. Same as in Table 1, with illuminator irradiation by eight beams.

Sector No.	E_{las}/J		$\langle I_a \rangle / 10^{14}$ W cm^{-2}		$\langle \eta \rangle$		T_X/eV		Sector positions
	$f = 0.1$	$f = 0.03$	$f = 0.1$	$f = 0.03$	$f = 0.1$	$f = 0.03$	$f = 0.1$	$f = 0.03$	
0	120	341					190	171	Openings
1	207	137	5.3	3.5	0.76	0.43	229	193	Primary laser spots on cylindrical surface coated with a 2-μm thick Au layer
2	185	120	4.8	3.1	0.7	0.38	226	190	
3	185	120	4.8	3.1	0.7	0.39	226	190	
4	207	137	5.3	3.5	0.76	0.43	229	193	
5	205	135	6.7	4.4	0.72	0.41	240	198	
6	178	113	6	3.8	0.66	0.38	236	194	
7	178	113	6	3.8	0.66	0.38	236	194	
8	205	135	6.7	4.4	0.72	0.4	240	198	
9	14	13.3	0.11	0.1	0.03	0.023	188	166	Front end face (1.8-μm thick Au layer)
10	3.8	3.6	0.026	0.025	0.05	0.015	143	138	Rear end face (50-μm thick Al layer)
11	316	635	0.65	1.3	0.77	0.55	190	191	Cylindrical surface beyond primary spots (2-μm thick Au layer)
12	0.36	0.34	0.03	0.029	0.07	0.02	143	138	Rear end face (50-μm thick Al layer)
13	0.22	0.17	0.044	0.035	0.06	0.015	143	138	
	E_L = 2003 J	E_L = 2003 J							

drawings that follow are given for $f = 0.03$. (The results of simulations for $f = 0.1$ are given in Tables 1–4.)

The high-intensity laser irradiation generates SWs, which propagate through the sample under investigation. In the simulations using the SND-LIRA code we determined the parameters of SWs in a plane aluminium sample. According to Ref. [1], in a 50-μm-thick aluminium sample the SW stationarity condition is fulfilled, which is required for carrying out correct measurements of its characteristics. Therefore, in what follows we analyse the parameters of SWs after passage through the base aluminium layer 50 μm in thickness. Figures 3–6 show the SW characteristics (the front position, its velocity, and the pressure behind the front) as functions of time in the cases of introduction of $N = 2$, 4, 6, and 8 laser beams, respectively.

Figures 3 and 5 show the time dependences of SW parameters in the case of laser energy injection through the end face (the two- and six-beam irradiation schemes). The existence of secondary laser irradiation (owing to light reflection inside the illuminator from its cylindrical surface) results in SW enhancement only in the two-beam injection case (when there is no additional box wall heating by the six beams introduced through the side openings). We note that to an X-ray ray radiation temperature $T_X = 100$ eV in the box there corresponds an energy flux $S_X \approx 10^{13}$ W cm^{-2}, which is less than the laser energy fluxes (see Table 1). To determine the degree of the additional sample heating by laser radiation, we performed simulations in which the effect of scattered laser radiation was neglected (unmarked curves in Figs 3 and 5).

In experiments with the use of an additional thin (5 μm) aluminium layer, which were performed on the Iskra-5 facility, the SW velocity v_f was measured at 30±3.6 km s^{-1} after passage through the basic aluminium layer [1]. To make a comparison with the experiment, we carried out simulations with a laser energy $E_L = 850$ J introduced into the box [1]. The simulated data are shown with unmarked curves in Fig. 4. The calculated SW velocity after passage through a 50-μm-thick aluminium layer was equal to 30 km s^{-1} (for $f = 0.03$).

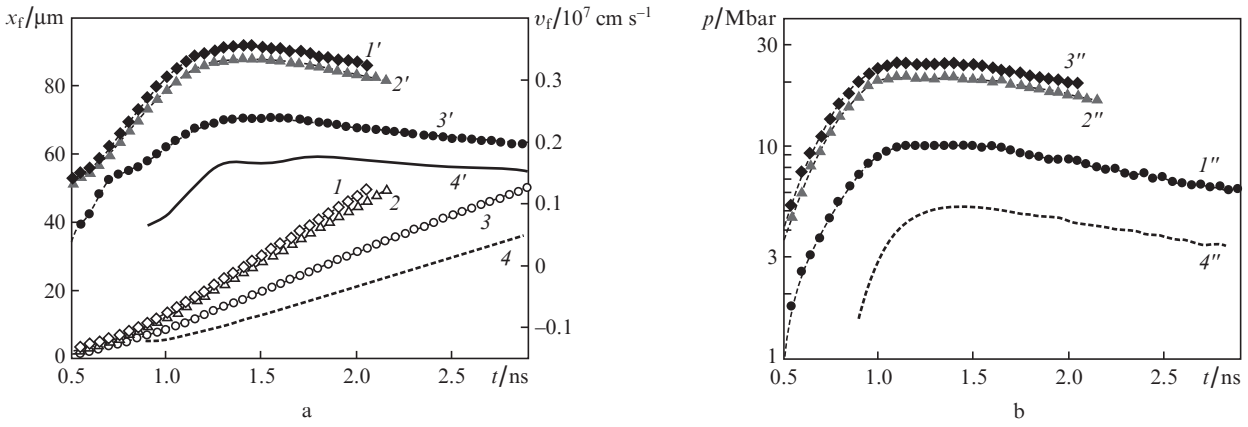

Figure 3. Time dependences of the position x_f of SW front travelling in an aluminium sample (*1–4*) and its instantaneous velocity v_f (*1′–4′*) (a), as well as the pressure p behind the SW front (*1″–4″*) (b) in the introduction of two laser beams, which were obtained in simulations with $f = 0.03$ for the zones of secondary irradiation of sectors 7 (*1*, *1′*, *1″*) and 6 (*2*, *2′*, *2″*), for the remaining part of the sample (*3*, *3′*, *3″*) and in the absence of additional laser irradiation of the sample (*4*, *4′*, *4″*).

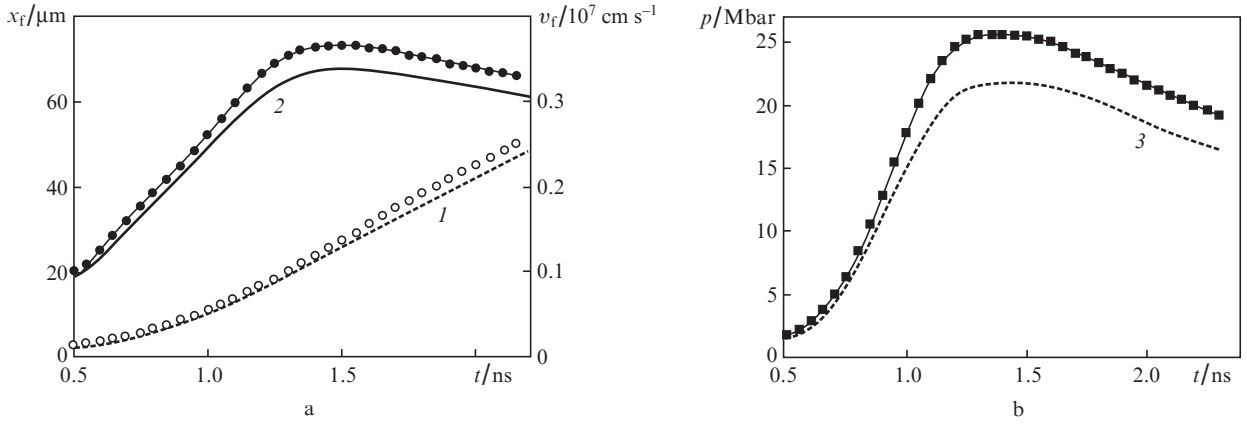

Figure 4. Time dependences of the position x_f of SW front travelling in an aluminium sample (*1*, ○) and its instantaneous velocity v_f (*2*, ●) (a), as well as the pressure p behind the SW front (*3*, ■) (b) in the case of four-beam illuminator irradiation for E_L = 1 kJ (points) and 850 J (curves) obtained in simulations with f = 0.03.

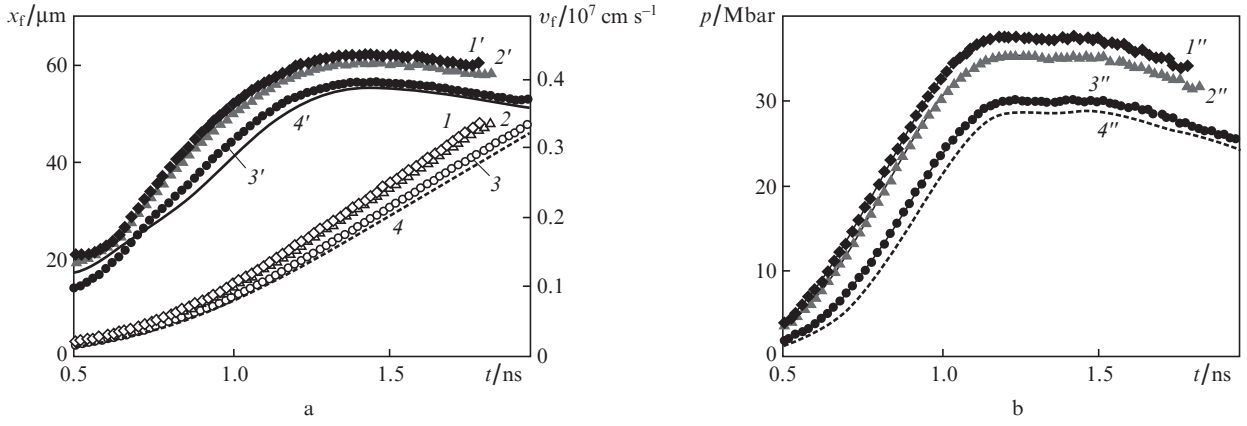

Figure 5. Same as in Fig. 3, but in the case of injection of six laser beams.

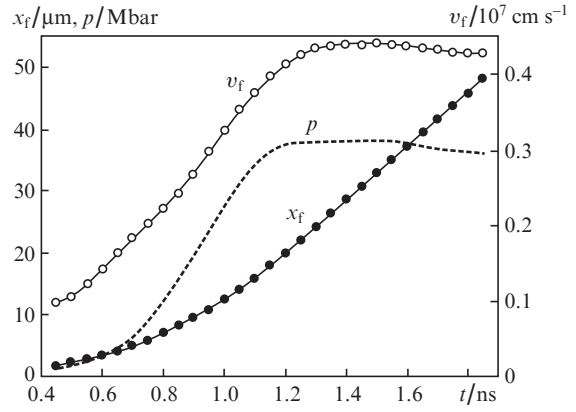

Figure 6. SW parameters in the case of injection of eight laser beams, which were obtained in simulations with f = 0.03.

Also given in Ref. [1] was the SW velocity for E_L = 1380 J. The SW velocity was measured at 35±1.6 km s^{-1}. In a simulation with f = 0.03 (the dashed curve in Fig. 5) we obtained a value v_f = 37 km s^{-1}. We note that the instant of SW exit was determined from the position of a laser mark, which introduces, in our opinion, some uncertainty in the measurement data.

3. Discussion of results

In the framework of the present work the SND-LIRA technique was employed to perform through numerical simulations of experiments with cylindrical illuminators in which the radiation temperature inside the box was calculated from the velocity of an SW in a 50-μm thick reference sample. In the simulations we determined the conditions of laser radiation absorption at the walls of the cylindrical box, the effective temperatures and the spectra of nonequilibrium X-ray radiation, and also investigated the conditions of SW generation under indirect (X-ray) action of quasi-thermal radiation on the surface of an aluminium sample.

We considered different versions of experiments with the use of N = 2, 4, 6, and 8 laser beams.

In the case of laser energy input through the end face (two beams are injected into the interior illuminator volume through the opening in its end face), it was shown that significant re-reflection of laser radiation inside the box results in the formation of zones of high-intensity secondary laser irradiation on the surface of the sample under investigation. In this case, the scattered laser radiation influences the sample under investigation, which substantially enhances the SW generated in it. The simulation data show that the uncontrolled effect of laser radiation on the sample is even stronger than the effect of X-ray radiation generated in the box in the case of two-beam illuminator irradiation.

In the scheme of six-beam laser irradiation of the box, the four additional beams are injected through the side openings and form the zones of high-intensity primary irradiation on the side (cylindrical) illuminator surface. The increase in X-ray radiation energy in the box lowers the influence of the scattered radiation of the two laser beams introduced through the end face opening. However, this influence is significant as before, and the results of measurement of the characteristics of the SW in the plane of beams propagation turn out to be distorted.

When four or eight beams are introduced through the four openings in the side illuminator surface, the laser radiation is absorbed primarily in the primary irradiation spots. In this case, the additional uncontrolled effect of the scattered radiation on the sample under investigation is eliminated, and it is possible to achieve a reasonably uniform X-ray illumination of its surface.

Our simulations showed that the difference between the cases of weak ($f = 0.1$) and strong ($f = 0.03$) electron heat transfer limitation manifests itself primarily in the zones of concentrated laser irradiation (both primary and secondary). The introduction of the stronger limitation ($f = 0.03$) was found to entail a significant imprisonment of heat in the tenuous plasma domain accessible to laser radiation propagation (the domain of laser corona). This has two consequences. First, the plasma heating results in a lower absorption of laser radiation in it. Second, the limitation of heat transfer to the denser supercritical plasma layers (X-ray corona) lowers the effective radiance temperature of the box walls in the zones of concentrated laser irradiation. This can be seen from the data collected in Tables 1–4.

The large number of experiments with indirect irradiation targets performed on Iskra-5 laser facility (the second iodine-laser harmonic with $\lambda = 0.66$ μm) permitted deriving the dependence (scaling) [1] of the effective X-ray radiation temperature T (in eV) in the box on the intensity I of laser radiation (in TW cm^{-2}) in the form

$$T = 60\,(0.35 I\tau^{1/2})^{0.29}, \qquad (4)$$

where τ is the laser pulse duration (in ns). The temperature of the radiation emanating from the openings, which was calculated by the SND-LIRA technique for electron thermal flux limiters $f = 0.1$ and 0.03, is compared with the measurement data in Fig. 7. One can see that the simulations are in better agreement with experimental data for the flux limiter $f = 0.03$. In the introduction of two beams, the simulation values of the X-ray radiation temperature lie below the scaling line. This is attributable to the fact that in this case the main absorption of laser radiation takes place in the secondary irradiation zones on the aluminium sample (see Fig. 1), whose effective radiance temperature is well below the temperature of the gold-coated box wall.

We emphasise that measurements of the spectrum of X-ray radiation emanating from the openings yield averaged temperature values, the radiation both of laser irradiation spots and of the box walls in the shadow region making their contribution. The conditions in concentrated laser irradiation zones are substantially changed on varying f from 0.03 to 0.1 (see Tables 1–4). The difference in averaged values is less pronounced, but is nevertheless appreciable. Therefore, by comparing the data of through simulations by the SND-LIRA technique with the measurement data it is possible to determine the electron thermal flux limiter f under the conditions of laser target experiments on the Iskra-5 facility.

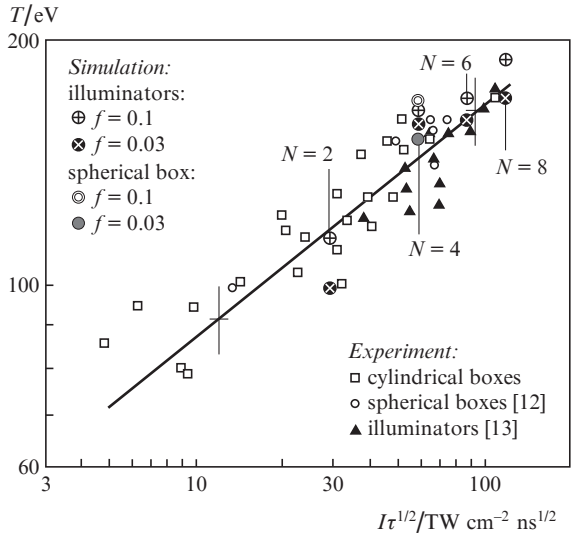

Figure 7. Comparison of the simulation temperature of the X-ray radiation emanating from the openings with the data of measurements on the Iskra-5 facility for a different number N of laser beams introduced into the box. The solid line represents the scaling (4).

Correct calculation of the X-ray radiation temperature in the box provides a possibility of calculating the SW velocity in an aluminium sample, which are consistent with the data of measurements (see Section 2).

4. Conclusions

This work outlines the results of numerical simulations of experiments on SW generation in a cylindrical illuminator which were performed on the Iskra-5 laser facility (the second harmonic of an iodine laser). The SND-LIRA technique was employed to carry out through numerical simulations of the dynamics of laser and X-ray radiation fields at the walls of a cylindrical converter box, as well as of the propagation of the SWs generated in the sample under investigation under heating by the high-intensity X-ray radiation.

An analysis of the simulation data suggests, first, that the scheme of illuminator irradiation with the use of two laser beams is unsatisfactory because of the undesirable irradiation of the sample under investigation by the scattered high-intensity laser radiation (see Fig. 2). The additional effect of scattered laser radiation on the sample under investigation takes place in experiments involving six laser beams as well, which may also distort the resultant experimental data. However, in this case the dominant effect is exerted on the sample by the quasi-equilibrium X-ray radiation generated in the box.

The experimental schemes with the injection of four or eight laser beams through four openings in the side illuminator surface are satisfactory from this point of view. On the one hand, they provide a high uniformity of X-ray irradiation of the sample under investigation and, on the other hand, they eliminate the effect of scattered laser radiation on the sample. In these cases, the effective X-ray radiation temperatures in the box amount to 150 and 170 eV, respectively.

The use of scaling function (4) permits matching the simulation X-ray radiation temperatures in the box to those measured experimentally for an electron thermal flux limiter $f = 0.03$. The value of this result consists in that the f value was determined for pulsed laser radiation of subnanosecond

duration with $\lambda = 0.66$ μm (the second harmonic of an iodine laser), for which absorption data are hardly available from the scientific literature. This is due to the fact that for inertial fusion experiments use is primarily made of the third harmonic of neodymium laser radiation ($\lambda = 0.35$ μm). The data for this wavelength obtained on the American laser facilities NOVA and OMEGA yield $f = 0.05$ for laser pulses of nanosecond duration [13, 14]. (In all cases the numerical interpretation of experiments was performed using the simple version of an average ion model for calculating nonequilibrium X-ray spectra.)

Finally, for $f = 0.03$ our simulations yield values of SW propagation velocity in aluminium, which coincide with the experimental ones.

References

1. Vatulin V.V., Zhidkov N.V., Kravchenko A.G. et al. *Fiz. Plazmy*, **36** (5), 447 (2010).
2. Bondarenko S.V., Dolgoleva G.V., Novikova E.A. *Voprosy Atomnoi Nauki i Tekhniki. Ser. Matematicheskoe Modelirovanie Fizicheskikh Protsessov*, (3-4), 15 (2007).
3. Bondarenko S.V., Dolgoleva G.V., Novikova E.A. *Kvantovaya Elektron.*, **37** (4), 372 (2007) [*Quantum Electron.*, **37** (4), 372 (2007)].
4. Sobol' I.M. *Chislennye metody Monte-Karlo* (Numerical Monte Carlo Methods) (Moscow: Nauka, 1973).
5. Bondarenko S.V., Novikova E.A. *Kvantovaya Elektron.*, **40** (5), 406 (2010) [*Quantum Electron.*, **40** (5), 406 (2010)].
6. Spitzer L. Jr., Härm R. *Phys. Rev.*, **89**, 977 (1953).
7. Malone R.C., McCrory R.L., Morse R.L. *Phys. Rev. Lett.*, **34**, 721 (1975).
8. Shvarts D., Delettrez J., McCrory R.L., Verdon C.P. *Phys. Rev. Lett.*, **47** (4), 247 (1981).
9. Silin V.P. *Zh. Eksp. Teor. Fiz.*, **106** (5(11)), 1398 (1994).
10. Shnittman J.D., Craxton R.S. *Phys. Plasmas*, **7** (7), 2964 (2000).
11. Bel'kov S.A., Dolgoleva G.V. *Voprosy Atomnoi Nauki i Tekhniki. Ser. Matematicheskoe Modelirovanie Fizicheskikh Protsessov*, (1), 59 (1992).
12. Annenkov V.I., Bessarab A.V., Vatulin V.V., et al. *Proc. XXIX ECLIM* (Madrid, Spain, 2006).
13. Rauffman R.L., Suter L.J., Darrow C.B., et al. *Phys. Rev. Lett.*, **73**, 2320 (1994).
14. Decker C., Turner R.E., Landen O.L., et al. *Phys. Rev. Lett.*, **79**, 1491 (1997).